
Semantic Correspondence with Transformers

Seokju Cho*
Yonsei University

Sunghwan Hong*
Korea University

Sangryul Jeon
Yonsei University

Yunsung Lee
Korea University

Kwanghoon Sohn
Yonsei University

Seungryong Kim†
Korea University

Abstract

We propose a novel cost aggregation network, called Cost Aggregation with Transformers (CATs), to find dense correspondences between semantically similar images with additional challenges posed by large intra-class appearance and geometric variations. Compared to previous hand-crafted or CNN-based methods addressing the cost aggregation stage, which either lack robustness to severe deformations or inherit the limitation of CNNs that fail to discriminate incorrect matches due to limited receptive fields, CATs explore global consensus among initial correlation map with the help of some architectural designs that allow us to exploit full potential of self-attention mechanism. Specifically, we include appearance affinity modelling to disambiguate the initial correlation maps and multi-level aggregation to benefit from hierarchical feature representations within Transformer-based aggregator, and combine with swapping self-attention and residual connections not only to enforce consistent matching, but also to ease the learning process. We conduct experiments to demonstrate the effectiveness of the proposed model over the latest methods and provide extensive ablation studies. Code and trained models will be made available at <https://github.com/SunghwanHong/CATs>.

1 Introduction

Establishing dense correspondences across semantically similar images can facilitate many Computer Vision applications, including semantic segmentation [44, 52, 34], object detection [27], and image editing [51, 28, 26, 23]. Unlike classical dense correspondence problems that consider visually similar images taken under the geometrically constrained settings [15, 18, 48, 17], semantic correspondence poses additional challenges from large intra-class appearance and geometric variations caused by the unconstrained settings of given image pair.

Recent approaches [40, 41, 43, 32, 35, 37, 29, 56, 45, 55, 49, 33] addressed these challenges by carefully designing deep convolutional neural networks (CNNs)-based models analogously to the classical matching pipeline [46, 39], feature extraction, cost aggregation, and flow estimation. Several works [22, 9, 35, 37, 45, 49] focused on the feature extraction stage, as it has been proven that the more powerful feature representation the model learns, the more robust matching is obtained [22, 9, 49]. However, solely relying on the matching similarity between features without any prior often suffers from the challenges due to ambiguities generated by repetitive patterns or background clutters [40, 22, 24]. On the other hand, some methods [40, 47, 41, 21, 24, 56] focused on flow estimation stage either by designing additional CNN as an ad-hoc regressor that predicts the parameters of a single global transformation [40, 41], finding confident matches from correlation maps [19, 24], or directly

*Equal contribution

†Corresponding author

feeding the correlation maps into the decoder to infer dense correspondences [56]. However, these methods highly rely on the quality of the initial correlation maps.

The latest methods [43, 35, 42, 20, 29, 25, 33] have focused on the second stage, highlighting the importance of cost aggregation. Since the quality of correlation maps is of prime importance, they proposed to refine the matching scores by formulating the task as optimal transport problem [45, 29], re-weighting matching scores by Hough space voting for geometric consistency [35, 37], or utilizing high-dimensional 4D or 6D convolutions to find locally consistent matches [43, 42, 25, 33]. Although formulated variously, these methods either use hand-crafted techniques that are neither learnable nor robust to severe deformations, or inherit the limitation of CNNs, e.g., limited receptive fields, failing to discriminate incorrect matches that are locally consistent.

In this work, we focus on the cost aggregation stage, and propose a novel cost aggregation network to tackle aforementioned issues. Our network, called Cost Aggregation with Transformers (CATs), is based on Transformer [59, 10], which is renowned for its global receptive field. By considering all the matching scores computed between features of input images globally, our aggregation networks explore global consensus and thus refine the ambiguous or noisy matching scores effectively.

Specifically, based on the observation that desired correspondence should be aligned at discontinuities with appearance of images, we concatenate an appearance embedding with the correlation map, which helps to disambiguate the correlation map within the Transformer. To benefit from hierarchical feature representations, following [24, 37, 56], we use a stack of correlation maps constructed from multi-level features, and propose to effectively aggregate the scores across the multi-level correlation maps. Furthermore, we consider bidirectional nature of correlation map, and leverage the correlation map from both directions, obtaining reciprocal scores by swapping the pair of dimensions of correlation map in order to allow global consensus in both perspective. With all these combined, we provide residual connections around aggregation networks in order to ease the learning process.

We demonstrate our method on several benchmarks [36, 11, 12]. Experimental results on various benchmarks prove the effectiveness of the proposed model over the latest methods for semantic correspondence. We also provide an ablation study to validate and analyze components in CATs.

2 Related Work

Semantic Correspondence. Methods for semantic correspondence generally follow the classical matching pipeline [46, 39], including feature extraction, cost aggregation, and flow estimation. Most early efforts [7, 28, 11] leveraged the hand-crafted features which are inherently limited in capturing high-level semantics. Though using deep CNN-based features [5, 22, 40, 41, 21, 47, 24] has become increasingly popular thanks to their invariance to deformations, without a means to refine the matching scores independently computed between the features, the performance would be rather limited.

To alleviate this, several methods focused on flow estimation stage. Rocco et al. [40, 41] proposed an end-to-end network to predict global transformation parameters from the matching scores, and their success inspired many variants [47, 21, 23]. RTNs [21] obtain semantic correspondences through an iterative process of estimating spatial transformations. DGC-Net [32] and Semantic-GLU-Net [56] utilize a CNN-based decoder to directly find correspondence fields. PDC-Net [57] proposed a flexible probabilistic model that jointly learns the flow estimation and its uncertainty. Arguably, directly regressing correspondences from the initial matching scores highly relies on the quality of them.

Recent numerous methods [43, 35, 37, 29, 45, 49, 33] thus have focused on cost aggregation stage to refine the initial matching scores. Among hand-crafted methods, SCOT [29] formulates semantic correspondence as an optimal transport problem and attempts to solve two issues, namely many to one matching and background matching. HPF [35] first computes appearance matching confidence using hyperpixel features and then uses Regularized Hough Matching (RHM) algorithm for cost aggregation to enforce geometric consistency. DHPF [37], that replaces feature selection algorithm of HPF [35] with trainable networks, also uses RHM. However, these hand-crafted techniques for refining the matching scores are neither learnable nor robust to severe deformations. As learning-based approaches, NC-Net [43] utilizes 4D convolution to achieve local neighborhood consensus by finding locally consistent matches, and its variants [42, 25] proposed more efficient methods. GOCor [55] proposed aggregation module that directly improves the correlation maps. GSF [20] formulated pruning module to suppress false positives of correspondences in order to refine the

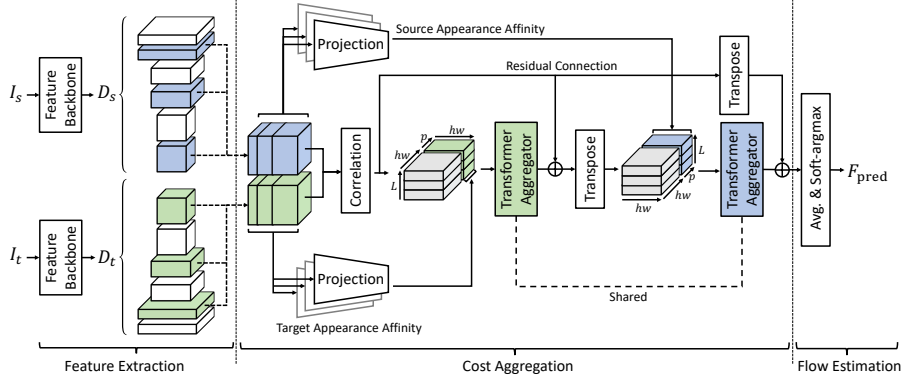


Figure 1: **Overall network architecture.** Our networks consist of feature extraction, cost aggregation, and flow estimation modules. We first extract multi-level dense features and construct a stack of correlation maps. We then concatenate with embedded features and feed into the Transformer-based cost aggregator to obtain a refined correlation map. The flow is then inferred from the refined map.

initial correlation maps. CHM [33] goes one step further, proposing a learnable geometric matching algorithm which utilizes 6D convolution. However, they are all limited in the sense that they inherit limitation of CNN-based architectures, which is local receptive fields.

Transformers in Vision. Transformer [59], the *de facto* standard for Natural Language Processing (NLP) tasks, has recently imposed significant impact on various tasks in Computer Vision fields such as image classification [10, 53], object detection [3, 60], tracking and matching [50, 49]. ViT [10], the first work to propose an end-to-end Transformer-based architecture for the image classification task, successfully extended the receptive field, owing to its self-attention nature that can captures global relationship between features. LoFTR [49] uses cross and self-attention module to refine the feature maps conditioned on both input images, and formulate the hand-crafted aggregation layer with dual-softmax [43, 58] and optimal transport [45] to infer correspondences. Unlike this, for the first time, we propose a Transformer-based cost aggregation module.

3 Methodology

3.1 Motivation and Overview

Let us denote a pair of images, i.e., source and target, as I_s and I_t , which represent semantically similar images, and features extracted from I_s and I_t as D_s and D_t , respectively. Here, our goal is to establish a dense correspondence field $F(i)$ between two images that is defined for each pixel i , which warps I_t towards I_s .

Estimating the correspondence with sole reliance on matching similarities between D_s and D_t is often challenged by the ambiguous matches due to the repetitive patterns or background clutters [40, 22, 24]. To address this, numerous methods proposed cost aggregation techniques that focus on refining the initial matching similarities either by formulating the task as optimal transport problem [45, 29], using regularized Hough matching to re-weight the costs [35, 37], or 4D or 6D convolutions [43, 25, 42, 33]. However, these methods either use hand-crafted techniques that are weak to severe deformations, or fail to discriminate incorrect matches due to limited receptive fields.

To overcome these, we present Transformer-based cost aggregation networks that effectively integrate information present in all pairwise matching costs, dubbed CATs, as illustrated in Fig. 1. As done widely in other works [40, 43, 48, 32, 35], we follow the common practice for feature extraction and cost computation. In the following, we first explain feature extraction and cost computation, and then describe several critical design choices we made for effective aggregation of the matching costs.

3.2 Feature Extraction and Cost Computation

To extract dense feature maps from images, we follow [24, 35, 37] that use multi-level features for construction of correlation maps. We use CNNs that produce a sequence of L feature maps, and D^l

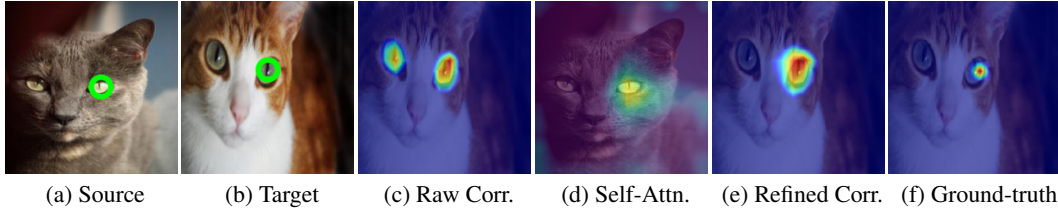


Figure 2: **Visualization of correlation map and self-attention:** (a) source image, (b) target image, (c) raw correlation map, (d) self-attention, (e) refined correlation map, and (f) ground-truth, which are bilinearly upsampled. The visualization proves that CATs successfully aggregates the costs by integrating the surrounding information of the query, represented as green circle in the source.

represents a feature map at l -th level. As done in [35], we use different combination of multi-level features depending on the dataset trained on, e.g., PF-PASCAL [12] or SPair-71k [36]. Given a sequence of feature maps, we resize all the selected feature maps to $\mathbb{R}^{h \times w \times c}$, with height h , width w , and c channels. The resized features then undergo $l-2$ normalization.

Given resized dense features D_s and D_t , we compute a correlation map $\mathcal{C} \in \mathbb{R}^{hw \times hw}$ using the inner product between features: $\mathcal{C}(i, j) = D_t(i) \cdot D_s(j)$ with points i and j in the target and source features, respectively. In this way, all pairwise feature matches are computed and stored. However, raw matching scores contain numerous ambiguous matching points as exemplified in Fig. 2, which results inaccurate correspondences. To remedy this, we propose cost aggregation networks in the following that aim to refine the ambiguous or noisy matching scores.

3.3 Transformer Aggregator

Renowned for its global receptive fields, one of the key elements of Transformer [59] is the self-attention mechanism, which enables finding the correlated input tokens by first feeding into scaled dot product attention function, normalizing with Layer Normalization (LN) [1], and passing the normalized values to a MLP. Several works [10, 3, 60, 49] have shown that given images or features as input, Transformers [59] integrate the global information in a flexible manner by learning to find the attention scores for all pairs of tokens.

In this paper, we leverage the Transformer [59] to integrate the matching scores to discover global consensus by considering global context information. Specifically, we obtain a refined cost \mathcal{C}' by feeding the raw cost \mathcal{C} to the Transformer \mathcal{T} , consisting of self-attention, LN, and MLP modules:

$$\mathcal{C}' = \mathcal{T}(\mathcal{C} + E_{\text{pos}}), \quad (1)$$

where E_{pos} denotes positional embedding. The standard Transformer receives as input a 1D sequence of token embeddings. In our context, we reshape the correlation map \mathcal{C} into a sequence of vectors $\mathcal{C}(k) \in \mathbb{R}^{1 \times hw}$ for $k \in \{1, \dots, hw\}$. We visualize the refined correlation map with self-attention in Fig. 2, where the ambiguities are significantly resolved.

Appearance Affinity Modeling. When only matching costs are considered for aggregation, self-attention layer processes the correlation map itself disregarding the noise involved in the correlation map, which may lead to inaccurate correspondences. Rather than solely relying on raw correlation map, we additionally provide an appearance embedding from input features to disambiguate the correlation map aided by appearance affinity within the Transformer. Intuition behind is that visually similar points in an image, e.g., color or feature, have similar correspondences, as proven in stereo matching literature, e.g., Cost Volume Filtering (CVF) [15, 48].

To provide appearance affinity, we propose to concatenate embedded features projected from input features with the correlation map. We first feed the features D into linear projection networks, and then concatenate the output along corresponding dimension, so that the correlation map is augmented such that $[\mathcal{C}, \mathcal{P}(D)] \in \mathbb{R}^{hw \times (hw+p)}$, where $[\cdot]$ denotes concatenation, \mathcal{P} denotes linear projection networks, and p is channel dimension of embedded feature. Within the Transformer, self-attention layer aggregates the correlation map and passes the output to the linear projection networks to retain the size of original correlation \mathcal{C} .

Multi-Level Aggregation. As shown in [35, 32, 37, 56, 29], leveraging multi-level features allows capturing hierarchical semantic feature representations. Thus we also use multi-level features from

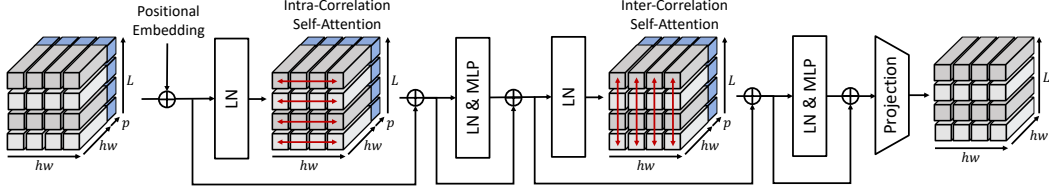


Figure 3: **Illustration of Transformer aggregator.** Given correlation maps \mathcal{C} with projected features, Transformer aggregation consisting of intra- and inter-correlation self-attention with LN and MLP refines the inputs not only across spatial domains but across levels.

different levels of convolutional layers to construct a stack of correlation maps. Each correlation map \mathcal{C}^l computed between D_s^l and D_t^l is concatenated with corresponding embedded features and fed into the aggregation networks. The aggregation networks now consider multiple correlations, aiming to effectively aggregates the matches by the hierarchical semantic representations.

As shown in Fig. 3, a stack of L augmented correlation maps, $[\mathcal{C}^l, \mathcal{P}(D^l)]_{l=1}^L \in \mathbb{R}^{hw \times (hw+p) \times L}$, undergo the Transformer aggregator. For each l -th augmented correlation map, we aggregate with self-attention layer across all the points in the augmented correlation map, and we refer this as *intra*-correlation self-attention. In addition, subsequent to this, the correlation map undergoes *inter*-correlation self-attention across multi-level dimensions. Contrary to HPF [35] that concatenates all the multi-level features and compute a correlation map, which disregards the level-wise similarities, within the inter-correlation layer of the proposed model, the similar matching scores are explored across multi-level dimensions. In this way, we can embrace richer semantics in different levels of feature maps, as shown in Fig. 4.

3.4 Cost Aggregation with Transformers

By leveraging the Transformer aggregator, we present cost aggregation framework with following additional techniques to improve the performance.

Swapping Self-Attention. To obtain a refined correlation map invariant to order of the input images and impose consistent matching scores, we argue that reciprocal scores should be used as aids to infer confident correspondences. As correlation map contains bidirectional matching scores, from both target and source perspective, we can leverage matching similarities from both directions in order to obtain more reciprocal scores as done similarly in other works [43, 24].

As shown in Fig. 1, we first feed the augmented correlation map to the aforementioned Transformer aggregator. Then we transpose the output, swapping the pair of dimensions in order to concatenate with the embedded feature from the other image, and feed into the subsequent another aggregator. Note that we share the parameters of the Transformer aggregators to obtain reciprocal scores. Formally, we define the whole process as following:

$$\begin{aligned} \mathcal{S} &= \mathcal{T}([\mathcal{C}^l, \mathcal{P}(D_t^l)]_{l=1}^L + E_{\text{pos}}), \\ \mathcal{C}' &= \mathcal{T}([\mathcal{S}^l]^T, \mathcal{P}(D_s^l)]_{l=1}^L + E_{\text{pos}}), \end{aligned} \quad (2)$$

where $\mathcal{C}^T(i, j) = \mathcal{C}(j, i)$ denotes swapping the pair of dimensions corresponding to the source and target images; \mathcal{S} denotes the intermediate correlation map before swapping the axis. Note that NC-Net [43] proposed a similar procedure, separately processing the correlation map and its transposed version and adding the outputs, which produces a correlation map invariant to the particular order of the input images. Unlike this, we process the correlation map serially, first aggregating one pair of dimensions and then further aggregating with respect to the other pair. In this way, the subsequent attention layer is given more consistent matching scores as an input, allowing further reduction of inconsistent matching scores.

Residual Connection. At the initial phase when the correlation map is fed into the Transformers, noisy score maps are inferred due to randomly-initialized parameters, which could complicate the learning process. To stabilize the learning process and provide a better initialization for the matching, we employ the residual connection. Specifically, we enforce the cost aggregation networks to estimate the residual correlation by adding residual connection around aggregation networks.

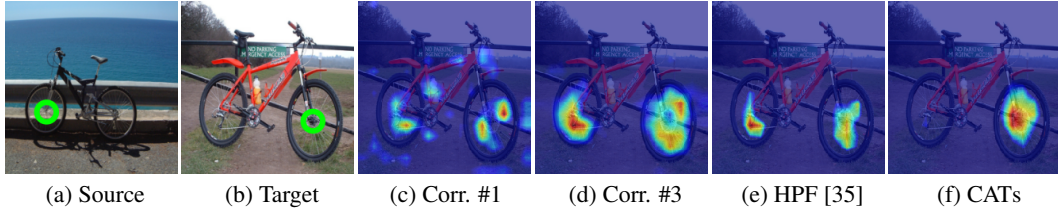


Figure 4: **Visualization of multi-level aggregation:** (a) source, (b) target images, (c), (d) multi-level correlation maps (e.g., $l = 1$ and $l = 3$), respectively, and final correlation maps by (e) HPF [35] and (f) CATs. Note that HPF and CATs utilize the same feature maps. Compared to HPF, CATs successfully embrace richer semantics in different levels of feature map.

3.5 Training

Data Augmentation. Transformer is well known for lacking some of inductive bias and its data-hungry nature thus necessitates a large quantity of training data to be fed [59, 10]. Recent methods [53, 54, 30] that employ the Transformer to address Computer Vision tasks have shown that data augmentation techniques guarantee performance boost. However, in correspondence task, the question of to what extent can data augmentation affect the performance has not yet been properly addressed. From the experiments, we have empirically found that data augmentation has positive impacts on performance in semantic correspondence with Transformers as reported in Section 4.4. To apply data augmentation [6, 2] with predetermined probabilities to input images at random. Specifically, 50% of the time, we randomly crop the input image, and independently for each augmentation function used in [6], we set the probability for applying the augmentation as 20%.

Training Objective. As in [35, 37, 33], we assume that the ground-truth keypoints are given for each pair of images. We first average the stack of refined correlation maps $C^l \in \mathbb{R}^{hw \times hw \times L}$ to obtain $C'' \in \mathbb{R}^{hw \times hw}$ and then transform it into a dense flow field F_{pred} using soft-argmax operator [24]. Subsequently, we compare the predicted dense flow field with the ground-truth flow field F_{GT} obtained by following the protocol of [35] using input keypoints. For the training objective, we utilize Average End-Point Error (AEPE) [32], computed by averaging the Euclidean distance between the ground-truth and estimated flow. We thus formulate objective function as $\mathcal{L} = \|F_{\text{GT}} - F_{\text{pred}}\|_2$.

4 Experiments

4.1 Implementation Details

For backbone feature extractor, we basically use ResNet-101 [14] pre-trained on ImageNet [8], and following [35], extract the features from the best subset layers. Other backbone features can also be used, which we analyze the effect of various backbone features in the following ablation study. For the hyper-parameters for Transformer encoder, we set the depth as 1 and the number of heads as 6. We resize the spatial size of the input image pairs to 256×256 and a sequence of selected features are resized to 16×16 . We use a learnable positional embedding [10], instead of fixed [59]. We implemented our network using PyTorch [38], and AdamW [31] optimizer with an initial learning rate of $3e-5$ for the CATs layers and $3e-6$ for the backbone features are used, which we gradually decrease during training. We will make our code publicly available in case of acceptance.

4.2 Experimental Settings

In this section, we conduct comprehensive experiments for semantic correspondence, by evaluating our approach through comparisons to state-of-the-art methods including CNNGeo [40], A2Net [47], WeakAlign [41], NC-Net [43], RTNs [21], SFNet [24], HPF [35], DCC-Net [16], ANC-Net [25], DHPF [37], SCOT [29], GSF [20], and CHMNet [33]. In Section 4.3, we first evaluate matching results on several benchmarks with quantitative measures, and then provide an analysis of each component in our framework in Section 4.4.

Datasets. SPair-71k [36] provides total 70,958 image pairs with extreme and diverse viewpoint, scale variations, and rich annotations for each image pair, e.g., keypoints, scale difference, truncation and occlusion difference, and clear data split. Previously, for semantic matching, most of the datasets

Table 1: **Quantitative evaluation on standard benchmarks [36, 11, 12].** Higher PCK is better. The best results are in bold, and the second best results are underlined. CATs[†] means CATs without fine-tuning feature backbone. *Feat.-level: Feature-level, FT. feat.: Fine-tune feature.*

| Methods | Feat.-level | FT. feat. | Aggregation | SPair-71k [36] | PF-PASCAL [12] | | | PF-WILLOW [11] | | |
|-------------------|-------------|-----------|-------------|-------------------------------------|--|-------------|-------------|---|-------------|-------------|
| | | | | PCK @ α_{bbox} 0.1 | PCK @ α_{img} 0.05 0.1 0.15 | | | PCK @ α_{bbox} 0.05 0.1 0.15 | | |
| WTA | Single | X | - | 25.7 | 35.2 | 53.3 | 62.8 | 24.7 | 46.9 | 59.0 |
| CNNGeo [40] | Single | X | - | 20.6 | 41.0 | 69.5 | 80.4 | 36.9 | 69.2 | 77.8 |
| A2Net [47] | Single | X | - | 22.3 | 42.8 | 70.8 | 83.3 | 36.3 | 68.8 | 84.4 |
| WeakAlign [41] | Single | X | - | 20.9 | 49.0 | 74.8 | 84.0 | 37.0 | 70.2 | 79.9 |
| RTNs [21] | Single | X | - | 25.7 | 55.2 | 75.9 | 85.2 | 41.3 | 71.9 | 86.2 |
| SFNet [24] | Multi | X | - | - | 53.6 | 81.9 | 90.6 | 46.3 | 74.0 | 84.2 |
| NC-Net [43] | Single | ✓ | 4D Conv. | 20.1 | 54.3 | 78.9 | 86.0 | 33.8 | 67.0 | 83.7 |
| DCC-Net [16] | Single | X | 4D Conv. | - | 55.6 | 82.3 | 90.5 | 43.6 | 73.8 | 86.5 |
| HPF [35] | Multi | - | RHM | 28.2 | 60.1 | 84.8 | 92.7 | 45.9 | 74.4 | 85.6 |
| GSF [20] | Multi | X | 2D Conv. | 36.1 | 65.6 | 87.8 | 95.9 | 49.1 | 78.7 | <u>90.2</u> |
| ANC-Net [25] | Single | X | 4D Conv. | - | - | 86.1 | - | - | - | - |
| DHPF [37] | Multi | X | RHM | 37.3 | <u>75.7</u> | 90.7 | <u>95.0</u> | 49.5 | 77.6 | 89.1 |
| SCOT [29] | Multi | - | OT-RHM | 35.6 | 63.1 | 85.4 | 92.7 | 47.8 | 76.0 | 87.1 |
| CHM [33] | Multi | ✓ | 6D Conv. | <u>46.3</u> | 80.1 | <u>91.6</u> | - | 52.7 | 79.4 | - |
| CATs [†] | Multi | X | Transformer | 42.4 | 67.5 | 89.1 | 94.9 | 46.6 | 75.6 | 87.5 |
| CATs | Multi | ✓ | Transformer | 49.9 | 75.4 | 92.6 | 96.4 | <u>50.3</u> | <u>79.2</u> | 90.3 |

Table 2: **Per-class quantitative evaluation on SPair-71k [36] benchmark.**

| Methods | aero. | bike | bird | boat | bott. | bus | car | cat | chai. | cow | dog | hors. | mbik. | pers. | plan. | shee. | tra. | tv | all |
|-------------------|-------------|-------------|-------------|-------------|-------------|-------------|-------------|-------------|-------------|-------------|-------------|-------------|-------------|-------------|-------------|-------------|-------------|-------------|-------------|
| CNNGeo [40] | 23.4 | 16.7 | 40.2 | 14.3 | 36.4 | 27.7 | 26.0 | 32.7 | 12.7 | 27.4 | 22.8 | 13.7 | 20.9 | 21.0 | 17.5 | 10.2 | 30.8 | 34.1 | 20.6 |
| A2Net [47] | 22.6 | 18.5 | 42.0 | 16.4 | 37.9 | 30.8 | 26.5 | 35.6 | 13.3 | 29.6 | 24.3 | 16.0 | 21.6 | 22.8 | 20.5 | 13.5 | 31.4 | 36.5 | 22.3 |
| WeakAlign [41] | 22.2 | 17.6 | 41.9 | 15.1 | 38.1 | 27.4 | 27.2 | 31.8 | 12.8 | 26.8 | 22.6 | 14.2 | 20.0 | 22.2 | 17.9 | 10.4 | 32.2 | 35.1 | 20.9 |
| NC-Net [43] | 17.9 | 12.2 | 32.1 | 11.7 | 29.0 | 19.9 | 16.1 | 39.2 | 9.9 | 23.9 | 18.8 | 15.7 | 17.4 | 15.9 | 14.8 | 9.6 | 24.2 | 31.1 | 20.1 |
| HPF [35] | 25.2 | 18.9 | 52.1 | 15.7 | 38.0 | 22.8 | 19.1 | 52.9 | 17.9 | 33.0 | 32.8 | 20.6 | 24.4 | 27.9 | 21.1 | 15.9 | 31.5 | 35.6 | 28.2 |
| SCOT [29] | 34.9 | 20.7 | 63.8 | 21.1 | 43.5 | 27.3 | 21.3 | 63.1 | 20.0 | 42.9 | 42.5 | 31.1 | 29.8 | 35.0 | 27.7 | 24.4 | 48.4 | 40.8 | 35.6 |
| DHPF [37] | 38.4 | 23.8 | 68.3 | 18.9 | 42.6 | 27.9 | 20.1 | 61.6 | 22.0 | 46.9 | 46.1 | 33.5 | 27.6 | 40.1 | 27.6 | 28.1 | 49.5 | 46.5 | 37.3 |
| CHM [33] | - | - | - | - | - | - | - | - | - | - | - | - | - | - | - | - | - | - | <u>46.3</u> |
| CATs [†] | <u>46.5</u> | <u>26.9</u> | <u>69.1</u> | <u>24.3</u> | <u>44.3</u> | <u>38.5</u> | <u>30.2</u> | <u>65.7</u> | 15.9 | <u>53.7</u> | <u>52.2</u> | <u>46.7</u> | <u>32.7</u> | 35.2 | <u>32.2</u> | <u>31.2</u> | <u>68.0</u> | <u>49.1</u> | 42.4 |
| CATs | 52.0 | 34.7 | 72.2 | 34.3 | 49.9 | 57.5 | 43.6 | 66.5 | 24.4 | 63.2 | 56.5 | 52.0 | 42.6 | 41.7 | 43.0 | 33.6 | 72.6 | 58.0 | 49.9 |

are limited to a small quantity with similar viewpoints and scales [11, 12]. As our network relies on Transformer which requires a large number of data for training, SPair-71k [36] makes the use of Transformer in our model feasible. we also consider PF-PASCAL [12] containing 1,351 image pairs from 20 categories and PF-WILLOW [11] containing 900 image pairs from 4 categories, each dataset providing corresponding ground-truth annotations.

Evaluation Metric. For evaluation on SPair-71k [36], PF-WILLOW [11], and PF-PASCAL [12], we employ a percentage of correct keypoints (PCK), computed as the ratio of estimated keypoints within the threshold from ground-truths to the total number of keypoints. Given predicted keypoint k_{pred} and ground-truth keypoint k_{GT} , we count the number of predicted keypoints that satisfy following condition: $d(k_{\text{pred}}, k_{\text{GT}}) \leq \alpha \cdot \max(H, W)$, where $d(\cdot)$ denotes Euclidean distance; α denotes a threshold which we evaluate on PF-PASCAL with α_{img} , SPair-71k and PF-WILLOW with α_{bbox} ; H and W denote height and width of the object bounding box or entire image, respectively.

4.3 Matching Results

For a fair comparison, we follow the evaluation protocol of [35] for SPair-71k, which our network is trained on the training split and evaluated on the test split. Similarly, for PF-PASCAL and PF-WILLOW, following the common evaluation protocol of [13, 21, 16, 35, 37], we train our network on the training split of PF-PASCAL [12] and then evaluate on the test split of PF-PASCAL [12] and PF-WILLOW [11]. All the results of other methods are reported under identical setting.

Table 1 summarizes quantitative results on SPair-71k [36], PF-PASCAL [12] and PF-WILLOW [11]. We note whether each method leverages multi-level features and fine-tunes the backbone features in order to ensure a fair comparison. We additionally denote the types of cost aggregation. Generally, our CATs outperform other methods over all the benchmarks. This is also confirmed by the results on SPair-71k, as shown in Table 2, where the proposed method outperforms other methods by large margin. Fig. 1 visualizes qualitative results for extremely challenging image pairs. We observe that compared to current state-of-the-art methods [29, 37], our method is capable of suppressing noisy scores and find accurate correspondences in cases with large scale and geometric variations.

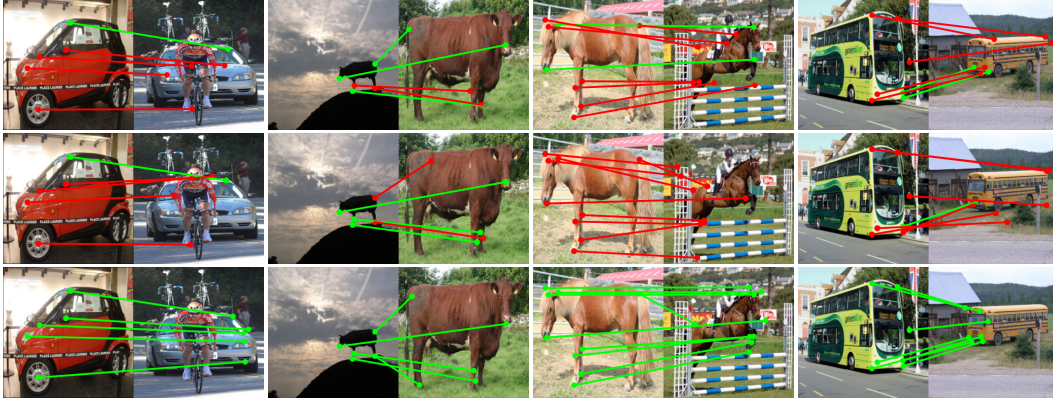


Figure 5: **Qualitative results on SPair-71k [36]:** (from top to bottom) keypoints transfer results by SCOT [29], DHPF [37], and CATs. Note that green and red line denotes correct and wrong prediction, respectively, with respect to the ground-truth.

It is notable that CATs generally report lower PCK on PF-WILLOW [11] compared to other state-of-the-art methods. This is because the Transformer is well known for lacking some of inductive bias. When we evaluate on PF-WILLOW, we infer with the model trained on the training split of PF-PASCAL, which only contains 1,351 image pairs, and as only relatively small quantity of image pairs is available within the PF-PASCAL training split, the Transformer shows low generalization power. This demonstrates that the Transformer-based architecture indeed requires a means to compensate for the lack of inductive bias, e.g., data augmentation.

4.4 Ablation Study

In this section we show an ablation analysis to validate critical components we made to design our architecture, and provide an analysis on use of different backbone features, and data augmentation. We train all the variants on the training split of SPair-71k [36] when evaluating on SPair-71k, and train on PF-PASCAL [12] for evaluating on PF-PASCAL. We measure the PCK, and each ablation experiment is conducted under same experimental setting for a fair comparison.

Network Architecture. Table 3 shows the analysis on key components in our architecture. There are four key components we analyze for the ablation study, including appearance modelling, multi-level aggregation, swapping self-attention, and residual connection. We first define the model without any of these as baseline, which simply feeds the correlation map into the self-attention layer. We evaluate on SPair-71k benchmark by progressively adding the each key component. From **I** to **V**, we observe consistent increase in performance when each component is added. **II** shows a large improvement in performance, which demonstrates that the appearance modelling enabled the model to refine the ambiguous or noisy matching scores. Although relatively small increase in PCK for **III**, it proves that the proposed model successfully aggregates the multi-level correlation maps. Furthermore, **IV** and **V** show apparent increase, proving the significance of both components.

Feature Backbone. As shown in Table 4, we explore the impact of different feature backbones on the performance on SPair-71k [36] and PF-PASCAL [12]. We report the results of models with backbone networks frozen. The top two rows are models with DeiT-B [53], next two rows use DINO [4], and the rest use ResNet-101 [14] as backbone. Specifically, subscript *single* for DeiT-B and DINO, we use the feature map extracted at the last layer for the single-level, while for subscript

Table 3: **Ablation study of CATs.**

| Components | | SPair-71k $\alpha_{\text{bbox}} = 0.1$ |
|--------------|---------------------------|---|
| (I) | Baseline | 26.8 |
| (II) | + Appearance Modelling | 33.5 |
| (III) | + Multi-level Aggregation | 35.9 |
| (IV) | + Swapping Self-Attention | 38.8 |
| (V) | + Residual Connection | 42.4 |

Table 4: **Ablation study of feature backbone.**

| Feature Backbone | SPair-71k $\alpha_{\text{bbox}} = 0.1$ | PF-PASCAL $\alpha_{\text{img}} = 0.1$ |
|--|---|--|
| DeiT-B _{single} [53] | 32.1 | 76.5 |
| DeiT-B _{all} [53] | 38.2 | 87.5 |
| DINO w/ ViT-B/16 _{single} [4] | 39.5 | 88.9 |
| DINO w/ ViT-B/16 _{all} [4] | 42.0 | 88.9 |
| ResNet-101 _{single} [14] | 37.4 | 87.3 |
| ResNet-101 _{multi} [14] | 42.4 | 89.1 |

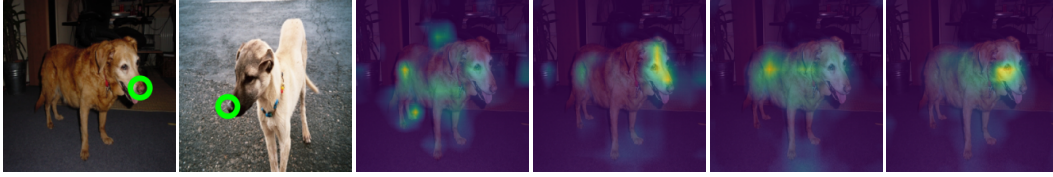


Figure 6: **Visualization of self-attention:** (from left to right) source and target images, and multi-level self-attentions. Note that each attention map attends different aspects, and CATs aggregates the cost leveraging hierarchical semantic representations.

all, every feature map from 12 layers is used for cost construction. For ResNet-101 subscript `single`, we use a single-level feature cropped at `conv4 - 23`, while for `multi`, we use the best layer subset provided by [35]. Summarizing the results, we observed that leveraging multi-level features showed apparent improvements in performance, proving effectiveness of multi-level aggregation introduced by our method. It is worth noting that DINO, which is more excel at dense tasks than DeiT-B, outperforms DeiT-B when applied to semantic matching. This indicates that fine-tuning the feature could enhance the performance. To best of our knowledge, we are the first to employ Transformer-based features for semantic matching. It would be an interesting setup to train an end-to-end Transformer-based networks, and we hope this work draws attention from the community and made useful for future works.

Data Augmentation. In Table 5, we compared the PCK performance between our variants and DHPF [37]. We note if the model is trained with augmentation. For a fair comparison, we evaluate both DHPF [37] and CATs trained on SPair-71k [36] using strong supervision, which assumes that the ground-truth keypoints are given. The results show that compared to DHPF, CNN-based networks, augmentation has a larger influence in performance in CATs. This demonstrates that not only we have satisfied data-hunger problem inherent in Transformers, but also found that applying augmentations for matching has positive effects.

Table 5: **Effects of augmentation.**

| | Augment. | SPair-71k $\alpha_{\text{bbox}} = 0.1$ |
|-----------|----------|---|
| DHPF [37] | ✗ | 37.3 |
| DHPF [37] | ✓ | 39.4 |
| CATs | ✗ | 43.5 |
| CATs | ✓ | 49.9 |

4.5 Analysis

Visualizing Self-Attention. We visualize the multi-level attention maps obtained from the Transformer aggregator. As shown in Fig. 6, the learned self-attention map at each level exhibits different aspect. With these self-attentions, our networks can leverage multi-level correlations to capture hierarchical semantic feature representations effectively.

Run-time. In Table 6, we show the run-time comparison to NC-Net [43], SCOT [29] and DHPF [37] with CATs. For a fair comparison, the run-times are obtained using a single NVIDIA GeForce RTX 2080 Ti GPU and Intel Core i7-10700 CPU. We measure the inference time for both the process without counting feature extraction, and the whole process. Thanks to Transformers’ fast computation nature, compared to other methods, our method is beyond compare.

Table 6: **Run-time comparison.** Inference time for aggregator is denoted by (\cdot) .

| | Aggregation | Run-time [ms] |
|-------------|-------------|-------------------|
| NC-Net [43] | 4D Conv. | 193.3 (166.1) |
| SCOT [29] | OT-RHM | 146.5 (81.6) |
| DHPF [37] | RHM | 57.7 (29.5) |
| CATs | Transformer | 34.5 (7.4) |

5 Conclusion

In this paper, we have proposed, for the first time, Transformer-based cost aggregation networks for semantic correspondence which enables aggregating the matching scores computed between input features, dubbed CATs. We have made several architectural designs in the network architecture, including appearance affinity modelling, multi-level aggregation, swapping self-attention, and residual correlation. We have shown that our method surpasses the current state-of-the-art in several benchmarks. Moreover, we have conducted extensive ablation studies to validate our choices and explore its capacity. A natural next step, which we leave for future work, is to examine how CATs

could extend its domain to tasks including 3-D reconstruction, semantic segmentation and stitching, and to explore self-supervised learning.

References

- [1] Jimmy Lei Ba, Jamie Ryan Kiros, and Geoffrey E Hinton. Layer normalization. *arXiv preprint arXiv:1607.06450*, 2016.
- [2] Alexander Buslaev, Vladimir I Iglovikov, Eugene Khvedchenya, Alex Parinov, Mikhail Druzhinin, and Alexandr A Kalinin. Albumentations: fast and flexible image augmentations. *Information*, 2020.
- [3] Nicolas Carion, Francisco Massa, Gabriel Synnaeve, Nicolas Usunier, Alexander Kirillov, and Sergey Zagoruyko. End-to-end object detection with transformers. In *ECCV*. Springer, 2020.
- [4] Mathilde Caron, Hugo Touvron, Ishan Misra, Hervé Jégou, Julien Mairal, Piotr Bojanowski, and Armand Joulin. Emerging properties in self-supervised vision transformers. *arXiv preprint arXiv:2104.14294*, 2021.
- [5] Christopher B Choy, JunYoung Gwak, Silvio Savarese, and Manmohan Chandraker. Universal correspondence network. *NeurIPS*, 29:2414–2422, 2016.
- [6] Ekin D Cubuk, Barret Zoph, Jonathon Shlens, and Quoc V Le. Randaugment: Practical automated data augmentation with a reduced search space. In *Proceedings of the IEEE/CVF Conference on Computer Vision and Pattern Recognition Workshops*, 2020.
- [7] Navneet Dalal and Bill Triggs. Histograms of oriented gradients for human detection. In *CVPR Workshops*, 2005.
- [8] Jia Deng, Wei Dong, Richard Socher, Li-Jia Li, Kai Li, and Li Fei-Fei. Imagenet: A large-scale hierarchical image database. In *CVPR*, 2009.
- [9] Daniel DeTone, Tomasz Malisiewicz, and Andrew Rabinovich. Superpoint: Self-supervised interest point detection and description. In *CVPR*, 2018.
- [10] Alexey Dosovitskiy, Lucas Beyer, Alexander Kolesnikov, Dirk Weissenborn, Xiaohua Zhai, Thomas Unterthiner, Mostafa Dehghani, Matthias Minderer, Georg Heigold, Sylvain Gelly, et al. An image is worth 16x16 words: Transformers for image recognition at scale. *arXiv preprint arXiv:2010.11929*, 2020.
- [11] Bumsub Ham, Minsu Cho, Cordelia Schmid, and Jean Ponce. Proposal flow. In *CVPR*, 2016.
- [12] Bumsub Ham, Minsu Cho, Cordelia Schmid, and Jean Ponce. Proposal flow: Semantic correspondences from object proposals. *IEEE transactions on pattern analysis and machine intelligence*, 2017.
- [13] Kai Han, Rafael S Rezende, Bumsub Ham, Kwan-Yee K Wong, Minsu Cho, Cordelia Schmid, and Jean Ponce. Snet: Learning semantic correspondence. In *ICCV*, 2017.
- [14] Kaiming He, Xiangyu Zhang, Shaoqing Ren, and Jian Sun. Deep residual learning for image recognition. In *CVPR*, 2016.
- [15] Asmaa Hosni, Christoph Rhemann, Michael Bleyer, Carsten Rother, and Margrit Gelautz. Fast cost-volume filtering for visual correspondence and beyond. *PAMI*, 2012.
- [16] Shuaiyi Huang, Qiuyue Wang, Songyang Zhang, Shipeng Yan, and Xuming He. Dynamic context correspondence network for semantic alignment. In *ICCV*, 2019.
- [17] Tak-Wai Hui, Xiaoou Tang, and Chen Change Loy. Liteflownet: A lightweight convolutional neural network for optical flow estimation. In *CVPR*, 2018.
- [18] Eddy Ilg, Nikolaus Mayer, Tonmoy Saikia, Margret Keuper, Alexey Dosovitskiy, and Thomas Brox. Flownet 2.0: Evolution of optical flow estimation with deep networks. In *CVPR*, 2017.
- [19] Sangryul Jeon, Seungryong Kim, Dongbo Min, and Kwanghoon Sohn. Parn: Pyramidal affine regression networks for dense semantic correspondence. In *ECCV*, 2018.
- [20] Sangryul Jeon, Dongbo Min, Seungryong Kim, Jihwan Choe, and Kwanghoon Sohn. Guided semantic flow. In *ECCV*. Springer, 2020.
- [21] Seungryong Kim, Stephen Lin, Sang Ryul Jeon, Dongbo Min, and Kwanghoon Sohn. Recurrent transformer networks for semantic correspondence. In *NeurIPS*, 2018.

- [22] Seungryong Kim, Dongbo Min, Bumsub Ham, Sangryul Jeon, Stephen Lin, and Kwanghoon Sohn. Fcss: Fully convolutional self-similarity for dense semantic correspondence. In *CVPR*, 2017.
- [23] Seungryong Kim, Dongbo Min, Somi Jeong, Sunok Kim, Sangryul Jeon, and Kwanghoon Sohn. Semantic attribute matching networks. In *CVPR*, 2019.
- [24] Junghyup Lee, Dohyung Kim, Jean Ponce, and Bumsub Ham. Sfnets: Learning object-aware semantic correspondence. In *CVPR*, 2019.
- [25] Shuda Li, Kai Han, Theo W Costain, Henry Howard-Jenkins, and Victor Prisacariu. Correspondence networks with adaptive neighbourhood consensus. In *CVPR*, 2020.
- [26] Jing Liao, Yuan Yao, Lu Yuan, Gang Hua, and Sing Bing Kang. Visual attribute transfer through deep image analogy. *arXiv:1705.01088*, 2017.
- [27] Tsung-Yi Lin, Piotr Dollár, Ross Girshick, Kaiming He, Bharath Hariharan, and Serge Belongie. Feature pyramid networks for object detection. In *CVPR*, 2017.
- [28] Ce Liu, Jenny Yuen, and Antonio Torralba. Sift flow: Dense correspondence across scenes and its applications. *IEEE transactions on pattern analysis and machine intelligence*, 33(5):978–994, 2010.
- [29] Yanbin Liu, Linchao Zhu, Makoto Yamada, and Yi Yang. Semantic correspondence as an optimal transport problem. In *CVPR*, 2020.
- [30] Ze Liu, Yutong Lin, Yue Cao, Han Hu, Yixuan Wei, Zheng Zhang, Stephen Lin, and Baining Guo. Swin transformer: Hierarchical vision transformer using shifted windows. *arXiv preprint arXiv:2103.14030*, 2021.
- [31] Ilya Loshchilov and Frank Hutter. Decoupled weight decay regularization. *arXiv:1711.05101*, 2017.
- [32] Iaroslav Melekhov, Aleksei Tiulpin, Torsten Sattler, Marc Pollefeys, Esa Rahtu, and Juho Kannala. Dgc-net: Dense geometric correspondence network. In *WACV*, 2019.
- [33] Juhong Min and Minsu Cho. Convolutional hough matching networks. *arXiv preprint arXiv:2103.16831*, 2021.
- [34] Juhong Min, Dahyun Kang, and Minsu Cho. Hypercorrelation squeeze for few-shot segmentation. *arXiv preprint arXiv:2104.01538*, 2021.
- [35] Juhong Min, Jongmin Lee, Jean Ponce, and Minsu Cho. Hyperpixel flow: Semantic correspondence with multi-layer neural features. In *ICCV*, 2019.
- [36] Juhong Min, Jongmin Lee, Jean Ponce, and Minsu Cho. Spair-71k: A large-scale benchmark for semantic correspondence. *arXiv preprint arXiv:1908.10543*, 2019.
- [37] Juhong Min, Jongmin Lee, Jean Ponce, and Minsu Cho. Learning to compose hypercolumns for visual correspondence. In *ECCV*, 2020.
- [38] Adam Paszke, Sam Gross, Soumith Chintala, Gregory Chanan, Edward Yang, Zachary DeVito, Zeming Lin, Alban Desmaison, Luca Antiga, and Adam Lerer. Automatic differentiation in pytorch. 2017.
- [39] James Philbin, Ondrej Chum, Michael Isard, Josef Sivic, and Andrew Zisserman. Object retrieval with large vocabularies and fast spatial matching. In *CVPR. IEEE*, 2007.
- [40] Ignacio Rocco, Relja Arandjelovic, and Josef Sivic. Convolutional neural network architecture for geometric matching. In *CVPR*, 2017.
- [41] Ignacio Rocco, Relja Arandjelović, and Josef Sivic. End-to-end weakly-supervised semantic alignment. In *CVPR*, 2018.
- [42] Ignacio Rocco, Relja Arandjelović, and Josef Sivic. Efficient neighbourhood consensus networks via submanifold sparse convolutions. In *ECCV*, 2020.
- [43] Ignacio Rocco, Mircea Cimpoi, Relja Arandjelović, Akihiko Torii, Tomas Pajdla, and Josef Sivic. Neighbourhood consensus networks. In *NeurIPS*, 2018.
- [44] Michael Rubinstein, Armand Joulin, Johannes Kopf, and Ce Liu. Unsupervised joint object discovery and segmentation in internet images. In *CVPR*, 2013.

- [45] Paul-Edouard Sarlin, Daniel DeTone, Tomasz Malisiewicz, and Andrew Rabinovich. Superglue: Learning feature matching with graph neural networks. In *CVPR*, 2020.
- [46] Daniel Scharstein and Richard Szeliski. A taxonomy and evaluation of dense two-frame stereo correspondence algorithms. *International journal of computer vision*, 2002.
- [47] Paul Hongsuck Seo, Jongmin Lee, Deunsol Jung, Bohyung Han, and Minsu Cho. Attentive semantic alignment with offset-aware correlation kernels. In *ECCV*, 2018.
- [48] Deqing Sun, Xiaodong Yang, Ming-Yu Liu, and Jan Kautz. Pwc-net: Cnns for optical flow using pyramid, warping, and cost volume. In *CVPR*, 2018.
- [49] Jiaming Sun, Zehong Shen, Yuang Wang, Hujun Bao, and Xiaowei Zhou. Loftr: Detector-free local feature matching with transformers. *arXiv preprint arXiv:2104.00680*, 2021.
- [50] Peize Sun, Yi Jiang, Rufeng Zhang, Enze Xie, Jinkun Cao, Xinting Hu, Tao Kong, Zehuan Yuan, Changhu Wang, and Ping Luo. Transtrack: Multiple-object tracking with transformer. *arXiv preprint arXiv:2012.15460*, 2020.
- [51] Richard Szeliski. Image alignment and stitching: A tutorial. *Foundations and Trends® in Computer Graphics and Vision*, 2006.
- [52] Tatsunori Tanaii, Sudipta N Sinha, and Yoichi Sato. Joint recovery of dense correspondence and cosegmentation in two images. In *CVPR*, 2016.
- [53] Hugo Touvron, Matthieu Cord, Matthijs Douze, Francisco Massa, Alexandre Sablayrolles, and Hervé Jégou. Training data-efficient image transformers and distillation through attention. *arXiv preprint arXiv:2012.12877*, 2020.
- [54] Hugo Touvron, Matthieu Cord, Alexandre Sablayrolles, Gabriel Synnaeve, and Hervé Jégou. Going deeper with image transformers. *arXiv preprint arXiv:2103.17239*, 2021.
- [55] Prune Truong, Martin Danelljan, Luc V Gool, and Radu Timofte. Gocor: Bringing globally optimized correspondence volumes into your neural network. In *NeurIPS*, 2020.
- [56] Prune Truong, Martin Danelljan, and Radu Timofte. Glu-net: Global-local universal network for dense flow and correspondences. In *CVPR*, 2020.
- [57] Prune Truong, Martin Danelljan, Luc Van Gool, and Radu Timofte. Learning accurate dense correspondences and when to trust them. *arXiv preprint arXiv:2101.01710*, 2021.
- [58] Michał J Tyszkiewicz, Pascal Fua, and Eduard Trulls. Disk: Learning local features with policy gradient. *arXiv preprint arXiv:2006.13566*, 2020.
- [59] Ashish Vaswani, Noam Shazeer, Niki Parmar, Jakob Uszkoreit, Llion Jones, Aidan N Gomez, Lukasz Kaiser, and Illia Polosukhin. Attention is all you need. *arXiv preprint arXiv:1706.03762*, 2017.
- [60] Xizhou Zhu, Weijie Su, Lewei Lu, Bin Li, Xiaogang Wang, and Jifeng Dai. Deformable detr: Deformable transformers for end-to-end object detection. *arXiv preprint arXiv:2010.04159*, 2020.

Appendix

Appendix A. More Implementation Details

Network Architecture Details. Given resized input images $I_s, I_t \in \mathbb{R}^{256 \times 256 \times 3}$, we conducted experiments using different feature backbone networks, including DeiT-B [53], DINO [4] and ResNet-101 [14]. For the ResNet-101_{multi} in the paper, we use the best layer subset [35] of (0,8,20,21,26,28,29,30) for SPair-71k, and (2,17,21,22,25,26,28) for PF-PASCAL and PF-WILLOW. We resized the spatial resolution of extracted feature maps to 16×16 . The extracted features undergo l_2 normalization and the correlation maps are constructed using dot products. Contrary to original Transformer [59] with encoder-decoder architecture, CATs is an encoder-only architecture. Within our Transformer aggregator, as explained in the paper, we concatenate the embedded features with correlation maps. We feed the resized features into the projection networks to reduce the dimension from c to 128, where c is the channel dimension of the feature. We then feed the augmented correlation map into the transformer encoder, which we use 1 encoder layer and 6 heads in multi-head attention layers. We then use soft-argmax function [24] with temperature $\tau = 0.02$ to infer a dense correspondence field.

Training Details. For training on both SPair-71k [36] and PF-PASCAL [12], we set the initial learning rate for CATs as $3e-5$ and backbone networks as $3e-6$. We then decrease the learning rate using multi-step learning rate decay [38]. We use a batch size of 32. We trained our networks using AdamW [31] with weight decay of 0.05. For data augmentation implementation, we implemented random cropping of image with probability set to 0.5, and used functions implemented by [2] as shown in Table 1.

Table 1: **Data Augmentation.**

| | Augmentation type | Probability |
|-------|--------------------------|-------------|
| (I) | ToGray | 0.2 |
| (II) | Posterize | 0.2 |
| (III) | Equalize | 0.2 |
| (IV) | Sharpen | 0.2 |
| (V) | RandomBrightnessContrast | 0.2 |
| (VI) | Solarize | 0.2 |
| (VII) | ColorJitter | 0.2 |

Appendix B. PyTorch-like Code

To demonstrate the simplicity of the approach, we provide PyTorch-like pseudo-code of CATs in Algorithm 1. In the main code, we feed correlation maps, source and target embeddings to the cost aggregation networks. Within the cost aggregation networks, we implement affinity modelling and swapping self-attention, and $\text{TransformerAgg}(\cdot)$ represents Transformer aggregator. Note that we use learnable positional embedding in Transformer aggregator instead of fixed. The entire code will be made available soon.

Appendix C. Additional Results

More Qualitative Results. We provide more comparison of CATs and other state-of-the-art methods on SPair-71k [36], PF-PASCAL [12], and PF-WILLOW [12]. We also present multi-head and multi-level attention visualization on SPair-71k in Fig 4, and multi-level aggregation in Fig 5.

Algorithm 1 CATs Pseudocode, PyTorch-like

```
for I1, I2, flow_GT in loader: # load a pair of images and ground-truth flow
    D1, D2 = feature_extraction(I1), feature_extraction(I2)
    # list of features interpolated to size of 16x16, followed by flatten operation
    correlation = []
    src_embed = []
    tgt_embed = []
    for src, tgt, proj in zip(D1, D2, Projections):
        correlation.append(cosine_similarity(l2norm(tgt), l2norm(src)) # compute cosine similarity
        src_embed.append(proj(src)) # compute embedded source feature
        tgt_embed.append(proj(tgt)) # compute embedded target feature

    refined_corr = CAT(torch.stack(correlation, 1), torch.stack(src_embed, 1), torch.stack(tgt_embed, 1))
    flow_pred = soft_argmax(refined_corr) # flow estimation

    L = EPE(flow_pred, flow_GT) # loss computation
    L.backward() # backward propagation
    update(CAT) # update parameters

def CAT(corr, src_feat, tgt_feat): # cost aggregation with transformers
    X = torch.cat((corr, tgt_feat), dim=3) # target appearance affinity
    X = nn.Linear(384, 256)(TransformerAgg(X)) # feed into the transformer aggregator
    # Retain original shape B x L x 256 x 256
    X = X + corr # residual connection

    X = X.transpose(-1, -2) # swapping self-attention

    X = torch.cat((X, src_feat), dim=3) # source appearance affinity
    X = nn.Linear(384, 256)(TransformerAgg(X)) # feed into the transformer aggregator
    X = X + corr.transpose(-1,-2) # residual connection

    return X.mean(1)

def TransformerAgg(x): # Transformer aggregator
    B, L, H, W = x.shape
    x = x + pos_embed
    x = x.flatten(0, 1)
    x = x + attn_intra(LayerNorm(x))
    x = x + MLP_intra(LayerNorm(x))
    # Intra-correlation self-attention

    x = x.view(B, L, H, W).transpose(1, 2).flatten(0, 1)
    x = x + attn_inter(LayerNorm(x))
    x = x.view(B, H, L, W).transpose(1, 2).flatten(0, 1)
    x = x + MLP_inter(LayerNorm(x))
    # Inter-correlation self-attention

    x = x.view(B, L, H, W)
    return x
```



Figure 1: **Qualitative results on SPair-71k [36]:** keypoints transfer results by (a) DHPF [37], (b) SCOT [29], and (c) CATs, and (d) ground-truth. Note that green and red line denotes correct and wrong prediction, respectively, with respect to the ground-truth.

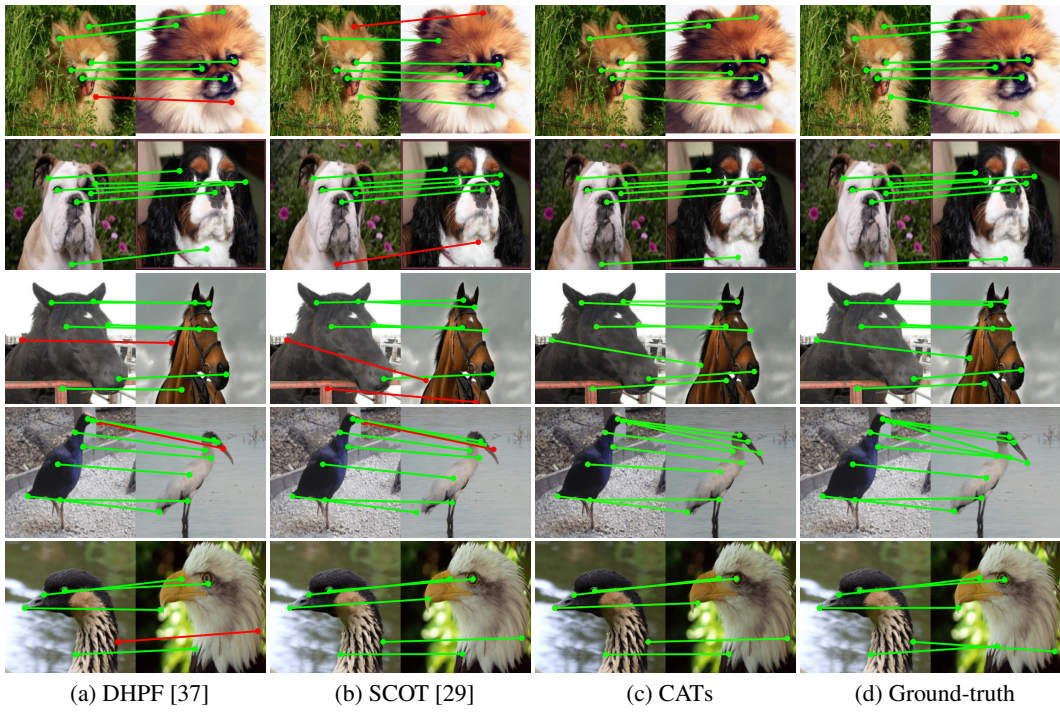


Figure 2: **Qualitative results on PF-PASCAL [12]**

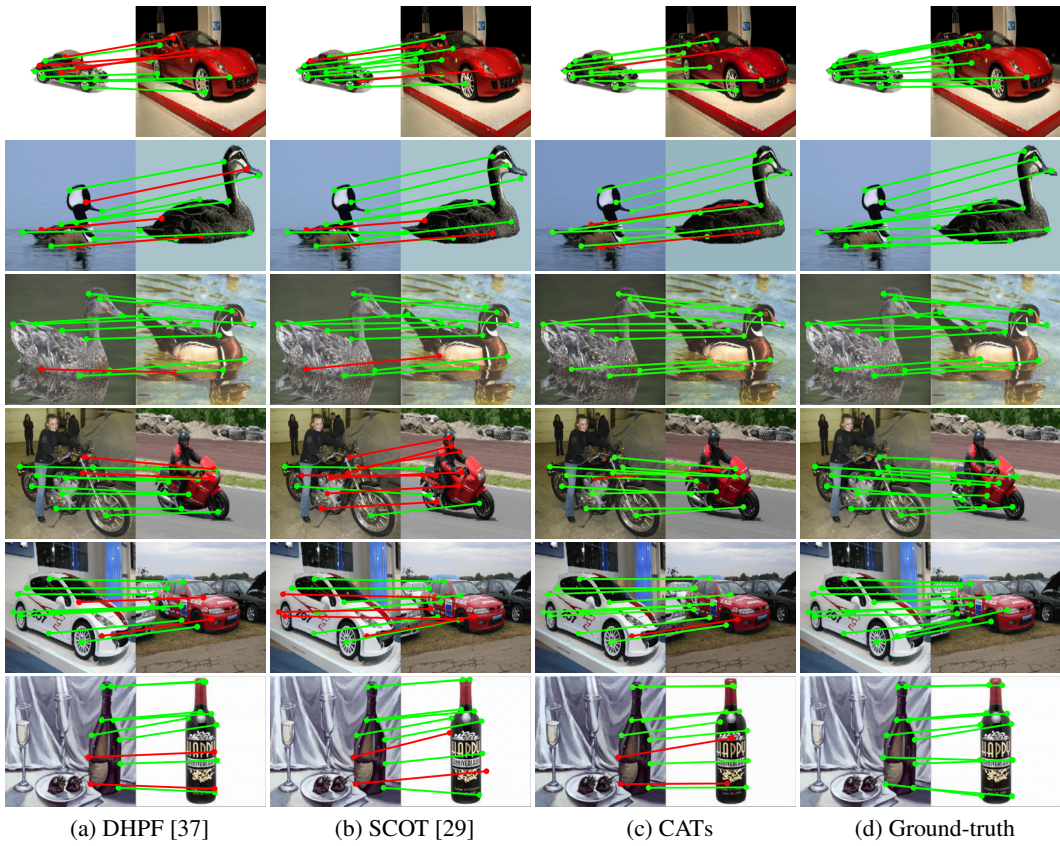


Figure 3: **Qualitative results on PF-WILLOW [11].**

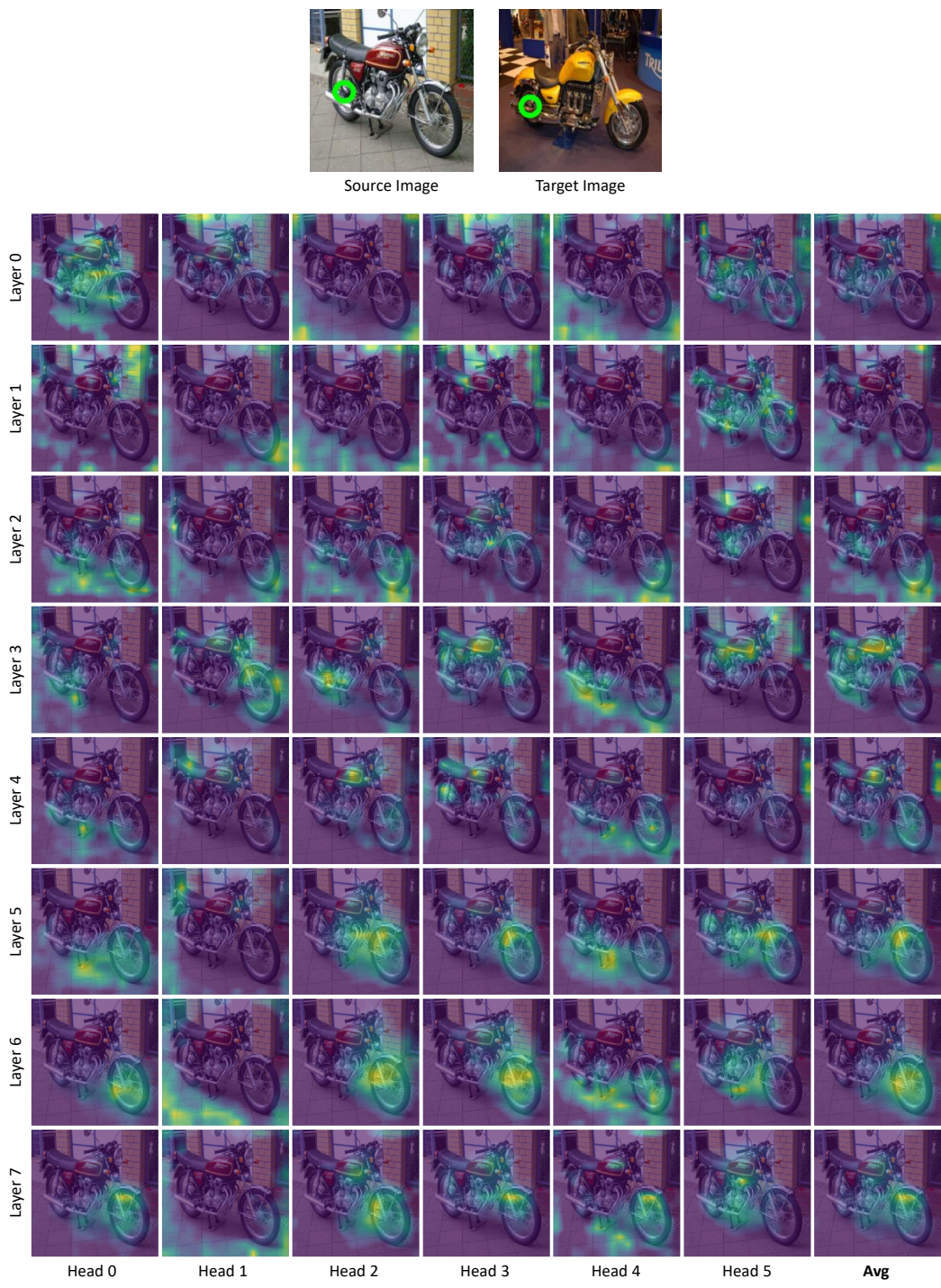


Figure 4: **Visualization of multi-head and multi-level self-attention.** Each head at l -th level layer, specifically among (0,8,20,21,26,28,29,30) layers of ResNet-101 [14] as in [35], attends different regions, which CATs successfully aggregates the multi-level correlation maps to infer reliable correspondences.



Figure 5: **Visualization of multi-level aggregation.** Each correlation refers to one of the (0,8,20,21,26,28,29,30) layers of ResNet-101, and our proposed method successfully aggregates the multi-level correlation maps.